Miner Deposita (2012) 47:623–632
DOI 10.1007/s00126-011-0396-x

ARTICLE

# Mantle-derived noble gases in ore-forming fluids of the granite-related Yaogangxian tungsten deposit, Southeastern China

**Rui-Zhong Hu · Xian-Wu Bi · Guo-Hao Jiang · Hong-Wei Chen · Jian-Tang Peng · You-Qiang Qi · Li-Yan Wu · Wen-Feng Wei**

Received: 13 March 2011 / Accepted: 19 December 2011 / Published online: 3 January 2012


**Abstract** More than 90% of the tungsten resources of China are in the Nanling region of South China, and the Yaogangxian vein deposit is the largest tungsten deposit in this region. The tungsten deposits have ages of 150–160 Ma, and are spatially, temporally and genetically related to granites which were previously believed to be produced by crustal anatexis. This paper provides He and Ar isotope data of fluid inclusions in pyrite and arsenopyrite from the Yaogangxian W veins. $^{3}He/^{4}He$ ratios range from 0.41 to 3.03 Ra (where Ra is the $^{3}He/^{4}He$ ratio of air=$1.39\times10^{-6}$), and $^{40}Ar/^{36}Ar$ ratios from 328 to 1,191. Moreover, there are excellent correlations between He and Ar isotopic compositions. The results suggest that the ore-forming fluids are a mixture between a crustal fluid containing atmospheric Ar and crustal $^{4}He$ and a fluid containing mantle components. It is likely that the former is a low temperature meteoric fluid, and the later is a fluid exsolved from the W-associated granitic magma, which formed by crustal melting induced by intrusion of a mantle-derived magma.

**Keywords** He and Ar isotopes · Ore-forming fluids · Tungsten deposit, granite · Mantle fluids · Nanling · China

Editorial handling: Hua and Zhou

R.-Z. Hu (✉) · X.-W. Bi · G.-H. Jiang · H.-W. Chen · J.-T. Peng · Y.-Q. Qi · L.-Y. Wu · W.-F. Wei
State Key Laboratory of Ore Deposit Geochemistry, Institute of Geochemistry, Chinese Academy of Sciences, Guiyang 550002, China
e-mail: huruizhong@vip.gyig.ac.cn

## Introduction

China is the world's largest producer of tungsten and also has the largest tungsten resources. More than 90% of the Chinese tungsten resources are in the Nanling region, South China (RGNTD 1985; Lu 1986), and the Yaogangxian deposit is the largest tungsten deposit of this region.

Previous studies have significantly advanced our understanding of the tungsten ore formation in the Nanling region. These deposits are usually of the quartz-wolframite vein type (e.g. RGNTD 1985; Lu 1986). They have ages of about 150–160 Ma (e.g. Mckee et al. 1987; Guo et al. 2007; Mao et al. 2007; Chen et al. 2008; Peng et al. 2006; Zhang et al. 2009), and are spatially and temporally related to granites, believed to be produced by crustal anatexis (Xu et al. 1984; Lu 1986; Wang et al. 1989; Hua et al. 2003, 2007, 2010; Chen et al. 2008; Wang 2008; Sun et al. 2009; Wang et al. 2009). The ore-forming fluids were considered to be mixtures of meteoric fluid with magmatic hydrothermal fluid derived from the W-associated granitic magma (Lu 1986; Zhang 1987; Chen 1992; Zhang et al.1997). However, it has been poorly constrained whether or not mantle components were involved in the genesis of the deposits.

Involvement of mantle-derived fluids in ore deposits can be traced using noble gas isotopes (Simmons et al. 1987; Turner and Stuart 1992; Turner et al. 1993; Stuart et al. 1995; Burnard et al. 1999; Hu et al. 1998, 2004, 2009). It is well known that $^{40}Ar/^{36}Ar$ can tell us the difference about atmospheric versus crust or mantle Ar, and that a factor of ~1,000–100 times difference between $^{3}He/^{4}He$ ratios of upper mantle (6–9Ra,

where Ra is the atmospheric $^{3}He/^{4}He$ ratio, $1.39\times10^{-6}$) and He produced in the crust (~0.05–0.01Ra) allows He to provide an unique insight into processes where mantle volatiles have been added to crustal fluids (Stuart et al. 1994, 1995; Baptiste and Fouquet 1996; Hu et al. 1998, 2004, 2009; Burnard et al. 1999; Kendrick et al. 2001, 2002a, b, 2005, 2011; Burnard and Polya 2004; Li et al. 2007a, b, c; Wu et al. 2011). This paper presents He and Ar isotopic analyses of fluid inclusions in pyrite and arsenopyrite from the Yaogangxian tungsten deposit. We use this dataset to discuss the origin of ore-forming fluids, thus the formation of the deposit and related granite.

## Geological background

South China is made up of the Yangtze Block in the northwest and the Cathaysian Block in the southeast (Fig. 1). To the north the late Paleozoic and early Mesozoic Qingling-Dabie orogenic belt lies between the Yangtze Block and the North China Block. To the west, the Yangtze Block is bounded by the Tibetan Plateau (Fig. 1).

The Yaogangxian tungsten deposit is located in the central Nanling region, northwestern part of the Cathaysian Block. The basement consists of weakly metamorphosed Precambrian folded strata, unconformably overlain by folded Paleozoic and Lower Mesozoic strata of shallow marine origin (Yan et al., 2003). Jurassic (early Yanshanian) granitic intrusions, consisting dominantly of biotite granites, two mica granites and muscovite granites, are widespread (Fig. 1). The intrusions have peraluminous composition and relatively high initial $^{87}Sr/^{86}Sr$ ratios of 0.710–0.735, and are commonly considered to be typical S-type granites (Xu et al. 1984; Lu 1986; Wang et al. 1989; Hua et al. 2003, 2007, 2010; Chen et al. 2008; Wang 2008; Sun et al. 2009; Wang et al. 2009). Numerous tungsten deposits, including Yaogangxian, Dajishan, Piaotang, Muziyuan, Xihuashan, Taoxikeng, were found in this region in the past decades. These deposits are usually of the quartz-wolframite vein type, and may also rich in Sn, Mo and Bi. They are spatially and temporally associated with the S-type granites.

In the Yaogangxian mining district, the stratigraphic sequence consists of Cambrian meta-sandstone and slate, unconformably overlain by Devonian and Carboniferous sandstone and limestone, and Jurassic sandstone. A two mica granitic pluton, with an exposed surface area of 1.2 $km^2$, intruded Cambrian and Devonian strata (Fig. 2). Rocks from the intrusion is felsic, with $SiO_2$ ranging from 74.0 to 78.0 wt%, $Al_2O_3$ from 11.5 to 14.1 wt%, $K_2O+Na_2O$ from 6.6 to 9.1 wt% and $K_2O/Na_2O>1$(Sun et al. 2009). U-Pb dating of zircon, and Ar-Ar and K-Ar dating of mica from the Dajishan, Piaotang, Muziyuan, Xihuashan, Taoxikeng granites indicate that the tungsten mineralization- related granites in the central Nanling region emplaced at ~155±5 Ma (Mckee et al. 1987; Jiang et al. 2004; Mao et al. 2007; Guo et al. 2007; Xiao et al. 2009; Zhang et al. 2006, 2009; Hua et al. 2003, 2010).

The Yaogangxian deposit consists of more than 200 ore veins. These veins are usually striking NNW to NWW (Fig. 2). Most ore veins occur along the northern contact zone between the granite and the sedimentary strata, and crosscut both lithologies. Individual veins are up to 1,200 m long,

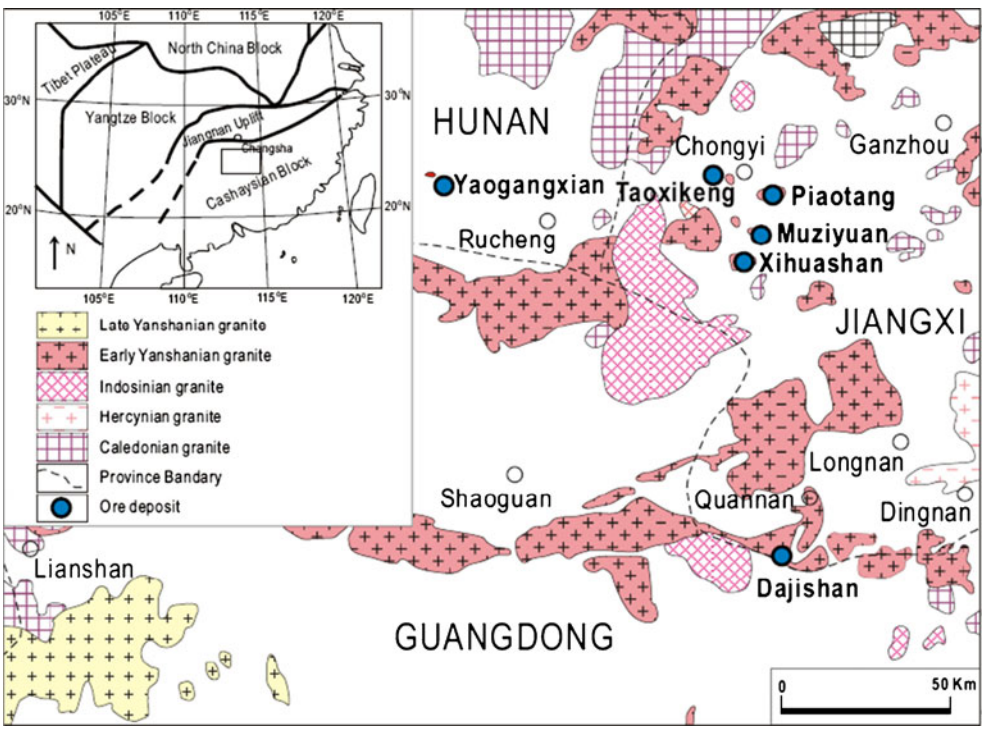


**Fig. 1** Sketch map of main tungsten deposits in the central Nanling region, South China. Modified after Chen et al. (2008) and Peng et al. (2006)

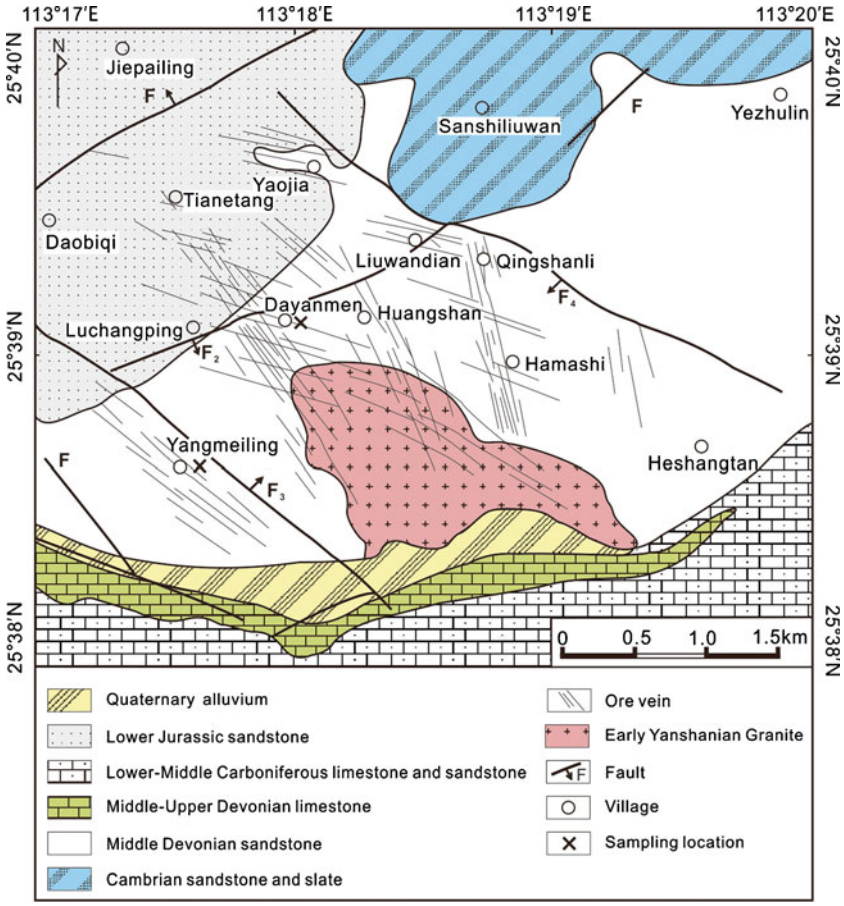


**Fig. 2** Simplified geological map of the Yaogangxian tungsten deposit, South China (modified from Peng et al. 2006)

1.5 m wide, and typically extend for 100 to 1,000 m downdip (Chen 1981). Generally, the veins increase in thickness with depth, but the number of veins decreases. Ore minerals in these veins are mainly wolframite and molybdenite with minor arsenopyrite, cassiterite, chalcopyrite, pyrite, bournonite and bismuthinite. Gangue minerals are predominately quartz with minor mica, feldspar, fluorite and calcite. Textures, crosscutting relationships, and mineral assemblages of the ores indicate that mineralization took place in four paragenetic stages which, from early to late, include a wolframite–molybdenite–quartz stage, a wolframite–cassiterite–quartz stage, a wolframite–sulfide–quartz stage, and a carbonate stage. The molybdenite Re-Os dating of the veins indicate that tungsten mineralization took place at 154.9±2.6 Ma (Peng et al. 2006), which almost corresponds to the ages of tungsten-bearing granites in the central Nanling region. The homogenization temperatures and salinity of fluid inclusions in quartz from various veins range from 180 to 360°C and from 1 to 15 wt.% NaCl equivalent, respectively (Ni 1994; Wang et al. 2007; Cao et al. 2009). Stable isotope compositions (Lu 1986; Zhang 1987; Chen 1992; Zhang et al.1997) are consistent with the ore-forming fluids being mixtures of meteoric fluid with magmatic hydrothermal fluid. The temperatures and salinity of the hydrothermal ore-forming fluids tend to decrease through the paragenetic sequence, while the proportions of meteoric fluid tend to increase from early to later stages. Samples of arsenopyrite and pyrite from the wolframite–cassiterite-quartz stage and the wolframite–sulfide–quartz stage were analyzed for He and Ar abundances and isotopes.

## Sampling and analytical methods

Samples were collected from underground workings. After the samples were crushed, mineral chips were hand-picked under a binocular microscope. Arsenopyrite separates of samples YGX57, YGX52 and YGX03 were selected from wolframite–cassiterite-quartz stage ores, and other analyzed sulfide separates were from wolframite–sulfide-quartz stage ores.

An all metal extraction line and mass spectrometer (GV 5400) at the Institute of Geochemistry, Chinese Academy of Sciences, Guiyang, was used. The analytical methods used here were similar to those described in Burnard et al. (1993) and Stuart et al. (1994, 1995). Approximately 500–1,000 mg of separated coarse (generally 0.5~1.5 mm, but the coarser the better) pyrite and arsenopyrite grains were cleaned ultrasonically in alcohol, dried, then loaded in on-line in vacuo crusher buckets. The samples were baked at ca.150°C on-lined with the ultra-high vacuum system for >24 h prior to analysis in order to remove adhered atmospheric gases. Gases were

released from the grains into the all metal extraction system by sequential crushing in modified Nupro type valves. The released gases were exposed to a titanium sponge furnace at 800°C for 20 min to remove the bulk of active gases (e.g. $H_2O$ and $CO_2$), and then exposed to two SAES Zr-Al getters (one at room temperature, the other at 450°C) for 10 min to further purify. He was separated from Ar using an activated charcoal cold finger at liquid $N_2$ temperature(−196°C) for 40–60 min to trap Ar. He and then Ar isotopes and abundances were analyzed on the GV 5400. Gas abundances were measured by peak-height comparison with known amounts of standard air from an air bottle. He and Ar abundances and isotopic ratios were calibrated against pipettes of 0.1 $cm^3$ STP air ($5.2\times10^{-7}$ $cm^3$ STP $^4He$ and $9.3\times10^{-4}$ $cm^3$ STP $^{40}Ar$). Procedural blanks were $<2\times10^{-10}cm^3STP^4He$ and $(2\sim4)\times10^{-10}cm^3STP^{40}Ar$, and constituted <1%of analyses. The blank is too low to affect calibration of the abundance measurement.

## Results and discussion

He and Ar isotope analyses of fluid inclusions in pyrite and arsenopyrite from the deposit are listed in Table 1. One disadvantage of the crushing analytical technique is the difficulty to separate different generations of fluid inclusions in the sample, and the results represent some averaging of all fluid inclusions crushed (Burnard and Polya 2004).

The concentrations of $^4He$ are $(0.1–14.5)\times10^{-6}cm^3STPg^{-1}$ and those of $^{40}Ar$ are $(0.6–22.0)\times10^{-7}cm^3STPg^{-1}$. The large variations of noble gas concentrations probably reflect variations in fluid inclusion abundance in minerals. Noble gas isotopic ratios are more consistent: $^3He/^4He$ ratios are 0.41–3.03 Ra (Ra represents the $^3He/^4He$ ratio of air, $1.39\times10^{-6}$), and $^{40}Ar/^{36}Ar$ ratios are 328–1,191.

## Helium

Whether the measured He isotopes of fluid inclusions reflect the original fluid composition depends on the extent of modifications by post-entrapment processes which may include addition of cosmogenic $^3He$ and in situ produced $^4He$, and He loss.

### Cosmogenic $^3He$

Post-crystallization production of $^3He$ within the mineral can occur by the interaction of cosmic rays with certain nuclei. This process is limited to the top 1.5 m of an exposed surface. Samples analyzed here were all collected from underground mine workings and cosmogenic $^3He$ production in mineral lattice and fluid inclusions can be ignored (Simmons et al. 1987; Stuart et al. 1995; Burnard et al. 1999).

### He loss

He loss from fluid inclusions is not likely to be significant because the samples analyzed are relatively young (~155 Ma) pyrite and arsenopyrite. Pyrite is known to be a suitable trap for noble gases (Stuart et al. 1994; Baptiste and Fouquet 1996; Burnard et al. 1999; Hu et al. 1998, 2004, 2009). It seems unlikely that arsenopyrite will be significantly different from pyrite (Burnard and Polya 2004). In fact, arsenopyrite has not been significantly affected by He loss because it has not been systematically depleted in $^4He/^{40}Ar$ relative to pyrite (Table 1).

### Effects of in situ produced $^4He$

Compared to fusion, a major advantage in using sequential crushing of minerals to extract noble gases is to preferentially release inclusion-trapped noble gases as opposed to those contained within the mineral lattice (Stuart et al. 1994). The amount of radiogenic $^4He$ released from a mineral lattice is dependent on the grain size of crushed minerals: the finer the minerals are crushed, the larger the surface area of the crushed grains and therefore the more radiogenic $^4He$ will be released from the mineral lattice (Stuart et al. 1995). Constant $^3He/^4He$ ratios during the crushing process (Table 1) suggest that negligible radiogenic $^4He$ was released from the mineral lattice and/or that He diffusion through pyrite is slow enough to prevent He loss during crushing.

Production of $^4He$ within the fluid inclusions is also unlikely to be significant. The difference between the $^3He/^4He$ ratios after subtracting in situ produced $^4He$ using U concentrations in the fluid is about the uncertainty of the measured value (<0.2 ppm U, 0 ppm Th, and a 155 Ma mineralization age were used to estimate the in situ $^4He$ production; U concentration is that of hydrothermal fluids of the Xiangshan U deposit (Hu et al. 2009), actual concentration is likely to be considerably less).

Therefore, it is likely that the measured He isotopic compositions of the samples listed in Table 1 could basically represent the "initial" values of fluid inclusions or ore-forming fluids of the deposit.

## Argon

Significant contributions of in situ produced $^{40}Ar$ from the mineral lattice to the measured $^{40}Ar/^{36}Ar$ ratios is thought unlikely due to the low diffusivity of Ar in pyrite and arsenopyrite (York et al. 1982; Smith et al. 2001; Burnard and Polya 2004) and the low K content of the analyzed minerals. Although in situ radiogenic $^{40}Ar$ growth in fluid inclusions from dissolved K or K-bearing minerals cannot be ruled out, the amount of in situ radiogenic $^{40}Ar$ in fluid

**Table 1** He and Ar isotopic compositions of inclusion-trapped fluid in pyrite and arsenopyrite from the Yaogangxian tungsten deposit

| Sample | Mineral | Crushing number | Weight[a] (g) | $^{4}He$[b] ($10^{-8}$ $cm^3$ STP) | $^{40}Ar$[b] ($10^{-8}$ $cm^3$ STP) | $^{3}He/^{4}He$ (Ra) | $^{40}Ar/^{36}Ar$ | $^{3}He/^{36}Ar$ ($10^{-3}$) | $^{40}Ar^{*}/^{4}He$ ($10^{-3}$) | $^{4}He$ ($cm^3$ STP $g^{-1}$) | $^{40}Ar$ ($cm^3$ STP $g^{-1}$) |
|---|---|---|---|---|---|---|---|---|---|---|---|
| ygx57 | Arsenopyrite | 1 | | 2.39±0.09 | 2.19±0.07 | 3.03±0.18 | 350±33 | 1.6±0.2 | 142.4±30.5 | | |
| | | 2 | | 9.19±0.33 | 6.79±0.22 | 2.22±0.12 | 332±21 | 1.4±0.1 | 81.0±24.5 | | |
| | | 3 | | 1.95±0.07 | –[d] | 2.82±0.19 | | | | | |
| | | Total[c] | 0.41 | 13.53±0.35 | | 2.45±0.09 | | | | 3.29E-07 | |
| ygx52 | Arsenopyrite | 1 | | 2.25±0.08 | –[d] | 2.58±0.18 | | | | | |
| | | 2 | | 7.00±0.25 | 1.88±0.06 | 2.04±0.11 | 600±48 | 6.4±0.5 | 136.1±10.1 | | |
| | | 3 | | 2.71±0.10 | –[d] | 2.39±0.16 | | | | | |
| | | Total[c] | 0.31 | 11.96±0.28 | | 2.22±0.08 | | | | 3.86E-07 | |
| ygx03 | Arsenopyrite | 1 | 0.28 | 3.59±0.13 | 1.75±0.06 | 2.41±0.15 | 404±26 | 2.8±0.2 | 131.2±16.7 | 1.28E-07 | 6.24E-08 |
| ygx43 | Pyrite | 1 | | 84.40±3.02 | 16.98±0.56 | 1.21±0.06 | 568±28 | 4.8±0.2 | 96.5±7.5 | | |
| | | 2 | | 79.20±2.82 | 16.82±0.55 | 1.46±0.08 | 595±30 | 5.7±0.3 | 106.8±8.0 | | |
| | | 3 | | 18.40±0.66 | 2.57±0.09 | 1.45±0.08 | 1,191±79 | 17.3±1.2 | 105.0±5.9 | | |
| | | Total[c] | 0.29 | 182.00±4.18 | 36.37±0.79 | 1.34±0.05 | 603±20 | 5.7±0.2 | 101.8±4.9 | 6.28E-06 | 1.25E-06 |
| ygx45 | Pyrite | 1 | | 32.00±1.14 | 14.24±0.47 | 0.92±0.05 | 388±19 | 1.1±0.1 | 106.0±15.1 | | |
| | | 2 | | 59.20±2.11 | 8.91±0.29 | 0.84±0.04 | 664±43 | 5.2±0.3 | 83.5±5.8 | | |
| | | 3 | | 32.10±1.14 | 5.67±0.19 | 0.89±0.05 | 569±40 | 4.0±0.3 | 84.9±6.5 | | |
| | | Total[c] | 0.35 | 123.30±2.66 | 28.82±0.58 | 0.87±0.03 | 480±16 | 2.5±0.1 | 89.7±5.1 | 3.52E-06 | 8.23E-07 |
| ygx48 | Pyrite | 1 | | 34.40±1.23 | 21.20±0.70 | 1.42±0.07 | 361±17 | 1.2±0.1 | 111.5±20.7 | | |
| | | 2 | | 68.20±2.43 | 15.40±0.51 | 1.53±0.08 | 594±30 | 5.6±0.3 | 113.5±8.5 | | |
| | | 3 | | 10.30±0.37 | 2.38±0.08 | 1.60±0.09 | 658±46 | 6.4±0.5 | 127.2±8.8 | | |
| | | Total[c] | 0.23 | 112.90±2.74 | 38.97±0.87 | 1.51±0.05 | 441±15 | 2.7±0.1 | 114.1±8.2 | 4.91E-06 | 1.69E-06 |
| ygx05 | Pyrite | 1 | 0.36 | 93.00±3.32 | –[d] | 0.41±0.02 | | | | 2.58E-06 | |
| ygx42 | Pyrite | 1 | 0.38 | 481.00±17.15 | 81.62±2.69 | 0.96±0.05 | 571±27 | 4.5±0.2 | 81.9±6.3 | 1.27E-05 | 2.15E-06 |
| ygx66 | Pyrite | 1 | 0.35 | 509.22±18.13 | 47.61±1.57 | 0.84±0.05 | 569±27 | 7.1±0.4 | 44.9±3.5 | 1.45E-05 | 1.36E-06 |
| ygx72 | Pyrite | 1 | 0.29 | 207.00±7.37 | 52.12±1.72 | 0.84±0.04 | 409±19 | 1.9±0.1 | 69.9±8.6 | 7.14E-06 | 1.80E-06 |
| ygx86 | Pyrite | 1 | 0.19 | 145.00±5.16 | 41.87±1.38 | 0.80±0.04 | 416±20 | 1.6±0.1 | 83.8±10.0 | 7.63E-06 | 2.20E-06 |
| ygx19 | Arsenopyrite | 1 | 0.43 | 47.30±1.68 | 6.28±0.21 | 1.25±0.06 | 433±25 | 5.7±0.3 | 42.1±4.6 | 1.10E-06 | 1.46E-07 |
| ygx27 | Arsenopyrite | 1 | 0.32 | 69.60±2.48 | 8.73±0.29 | 0.58±0.03 | 454±25 | 2.9±0.2 | 43.8±4.4 | 2.18E-06 | 2.73E-07 |
| ygx79 | Arsenopyrite | 1 | 0.34 | 21.60±0.77 | 7.17±0.24 | 1.31±0.07 | 361±19 | 2.0±0.1 | 60.2±11.1 | 6.35E-07 | 2.11E-07 |
| ygx61 | Arsenopyrite | 1 | 0.26 | 25.10±0.89 | 15.05±0.50 | 1.11±0.06 | 328±16 | 0.8±0.04 | 59.1±19.8 | 9.65E-07 | 5.79E-07 |

[a] Sample weights are the <100 μm fraction after crushing

[b] Errors quoted are at the 1$\sigma$ confidence level

[c] Totals are the sums of all crushes

[d] Not determined

[*] is non-atmospheric Ar

inclusions trapped in K-free minerals (such is the case in the present study) should be negligible (Turner and Wang 1992; Qiu 1996).

In general, the measured $^{40}Ar/^{36}Ar$ ratios will be lower than the true $^{40}Ar/^{36}Ar$ ratios of the fluids due to the contributions of atmospheric Ar (Burnard et al. 1999). Rigorous analytical procedures can minimize atmospheric Ar absorbed on the surfaces of the samples and the crushing apparatus, but cannot completely eliminate air-derived contaminants. As shown in Table 1, argon becomes increasingly radiogenic (higher $^{40}Ar/^{36}Ar$) as crushing (crush 1, crush 2 and crush 3 of a particular sample) proceeds, most likely due to decreasing contributions from a surface adsorbed atmospheric component as opposed to in situ decay of K to $^{40}Ar$. Therefore, the variation of $^{40}Ar/^{36}Ar$ ratios of a particular sample is more likely due to changes in proportions of atmospheric Ar that contaminates Ar derived from the fluids. In this instance, the only certain constraint on the true $^{40}Ar/^{36}Ar$ ratios of the inclusion-trapped fluids is that it must be higher than the highest value measured here (Burnard and Polya 2004). However, the $^{40}Ar/^{36}Ar$ variation of different samples may not be attributed entirely to air-contamination, and may reflect variable $^{40}Ar/^{36}Ar$ of the fluids. In fact, this is likely considering the $^{40}Ar^*/^4He$ is also variable (Table 1 and Fig. 4), and there is a correlation between $^{40}Ar/^{36}Ar$ and $^{40}Ar/^4He$ (not shown).

## Sources of He and Ar

Noble gases in inclusion-trapped fluids have three potential sources, notably air-saturated water, mantle and radiogenic isotopes produced within the crust [Turner et al. 1993]. Helium in the atmosphere is too low to exert a significant influence on He abundances and isotopic compositions of most crustal fluids (Marty et al. 1989; Stuart et al. 1994). As a result, He in ore-forming fluids of the deposits could have only two possible sources: mantle-derived He and radiogenic He produced in the crust (Turner et al. 1993). This is consistent with the $^3He/^{36}Ar$ ($0.8–17.3\times10^{-3}$) ratios in our samples which are five orders of magnitude higher than those of the atmosphere or air-saturated water ($\sim5\times10^{-8}$), indicating that He in the fluids that generated the Yaogangxian tungsten deposit was predominantly non-atmospheric in origin. The characteristic values of $^3He/^4He$ produced in the crust are 0.01– 0.05 Ra (Mamyrin and Tolstikhin 1984; Turner et al. 1993). As can be seen from Table 1, the $^3He/^4He$ ratios (0.41–3.03Ra) of the ore-forming fluids are much higher than those of the crust, but lower than those of the sub-continental mantle ($^3He/^4He\approx6$ Ra; Dunai and Baur 1995; Gautheron and Moreira 2002), demonstrating that the ore fluids contain mantle- and crustal-derived He. However, origin of argon in the fluids could be air-saturated water and mantle from the correlations between helium and argon isotopes (Figs. 3, 4). Therefore, the noble gases in the fluids are likely a mixture of three major end-member components, notably helium and argon from the mantle (here described as mantle fluid), argon in air-saturated water and radiogenic helium produced in the crust (here described together as crustal fluid).

### Crustal fluid: argon in air-saturated water and radiogenic helium produced in the crust

Air-saturated water (ASW) (meteoric or marine) is characterized by atmospheric He and Ar isotope compositions of $^{40}Ar/^{36}Ar=295.5$ and $^3He/^{36}Ar=5\times10^{-8}$ (Turner et al. 1993; Stuart et al. 1995; Burnard et al. 1999). The crustal fluid trapped in the fluid inclusions is probably best described as 'modified air-saturated water, MASW', i.e. air-saturated water with added crustal radiogenic components (much $^4He$ and little $^{40}Ar^*$). In general, $^3He/^{36}Ar$ ratios of the MASW fluids are unlikely to be changed, because both $^3He$ and $^{36}Ar$ are unradiogenic. Therefore, the trend in Fig. 3 can be extrapolated to the $^3He/^{36}Ar$ value of ASW ($5\times10^{-8}$), in order to calculate the MASW $^{40}Ar/^{36}Ar=302\pm18$ that is indistinguishable from air ($^{40}Ar/^{36}Ar=295.5$). The trend in Fig. 4 can also be extended to this modified air-saturated water. When $^3He/^4He$ ratios are smaller than 0.05 Ra (typical of crustally produced He), a $^4He/^{40}Ar^*$ ($^{40}Ar^*$ is non-atmospheric Ar, i.e. $^{40}Ar^*=^{40}Ar-[^{36}Ar.295.5]$) ratio of ca. 0.01~0.001 is obtained from the trend between $^3He/^4He$ and $^{40}Ar^*/^4He$ ratios (Fig. 4), significantly lower than the estimates of the likely instantaneous $^{40}Ar^*/^4He$ production ratio of the crust (≈0.2; Torgersen et al. 1988; Ballentine and Burnard 2002), suggesting preferential acquirement of $^4He$ relative to $^{40}Ar$ from crustal rocks. Previous studies have demonstrated that contemporary groundwaters commonly have low $^{40}Ar^*/^4He$ ratios due to preferential acquirement of $^4He$ relative to $^{40}Ar$ from crustal rocks, because of the higher closure temperature of Ar relative to He (Torgersen et

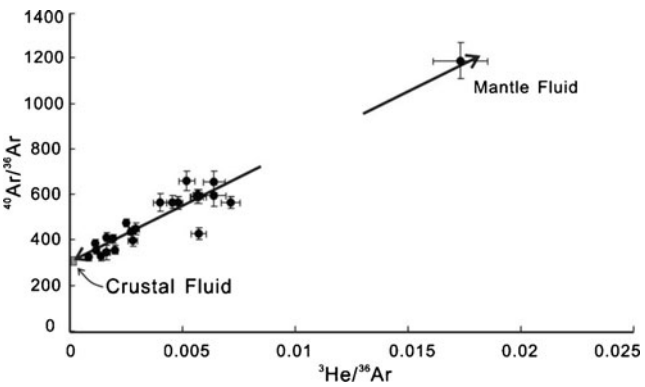


**Fig. 3** $^3He/^{36}Ar$ vs. $^{40}Ar/^{36}Ar$ plot of inclusion-trapped fluids from the Yaogangxian tungsten deposit. Least squares fitting of the data suggests that $^{40}Ar/^{36}Ar=50{,}359(\pm3{,}257)\ ^3He/^{36}Ar+302(\pm18)$ with $R^2=0.91$

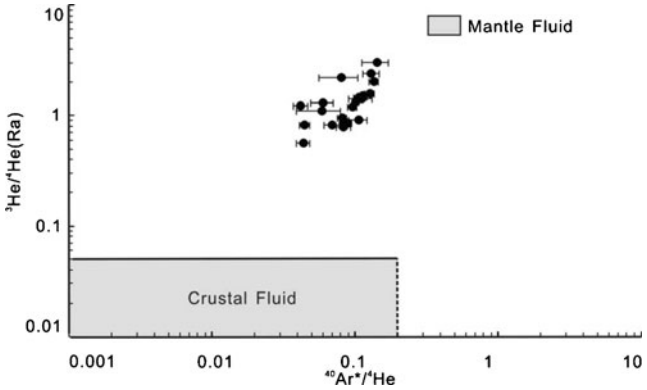


**Fig. 4** $^{40}$Ar*/$^4$He vs. $^3$He/$^4$He (Ra) plot of inclusion-trapped fluids from the Yaogangxian tungsten deposit

al. 1988; Ballentine and Burnard 2002). For the majority of minerals, the closure temperature of He is usually less than 200°C, whereas Ar is quantitatively retained in most minerals at 250°C (Lippolt and Weigel 1988; McDougall and Harrison 1988; Elliot et al. 1993). The MASW trapped in these samples preferentially acquired a large amount of He, but almost no Ar from crustal rocks, implying that the fluid interacted with crustal rocks in shallow aquifers for a long time, but at relatively low temperature (<200°C).

### Mantle fluid

Mantle-derived fluids are rich in $^3$He and poor in $^{36}$Ar (Turner et al. 1993). Consequently, the plausible source of the end-member with high $^3$He/$^4$He, high $^3$He/$^{36}$Ar and high $^{40}$Ar/$^{36}$Ar ratios (Figs. 3, 4) is derived from the mantle. Extrapolating the trend in Fig. 4 to a likely mantle $^3$He/$^4$He ratio of 6 Ra or so (the $^3$He/$^4$He value of sub-continental mantle: Dunai and Baur 1995; Gautheron and Moreira 2002) implies a $^{40}$Ar*/$^4$He ratio of 0.3–0.5. This value is generally consistent with $^{40}$Ar*/$^4$He ratios of the sub-continent mantle (0.33~0.56; Burnard et al. 1998).

Production of $^3$He in the crust is mainly controlled by the reaction $^6$Li(n,α)→$^3$H(β)→$^3$He (Mamyrin and Tolstikhin 1984; Morrison and Pine 1955). However, if in situ $^3$He production was responsible for the high $^3$He/$^4$He ratios measured in these samples, it would be extremely difficult to account for the excellent correlation between $^3$He/$^{36}$Ar and $^{40}$Ar/$^{36}$Ar, or between $^3$He/$^4$He and $^{40}$Ar*/$^4$He (Figs. 3 and 4) seen in these samples (see Hu et al. 2009 for more details). Therefore, we conclude that the high $^3$He/$^4$He ratios in the Yaogangxian tungsten deposit have resulted from a mantle component input.

## Mixing mechanism

It is clear that the ore-forming fluids for the Yaogangxian tungsten deposit are a mixture between a crustal fluid (MASW, i.e. atmospheric Ar and crustal $^4$He) and a fluid containing a mantle component. The mantle end-member in ore fluids could be unrelated to the granite and directly derived from mantle as suggested at Panasqueira (Burnard and Polya 2004). In Yaogangxian, However, the deposit is spatially and temporally associated with granite intrusion, and stable isotope studies are consistent with the ore-forming fluids being mixtures of meteoric fluid with magmatic hydrothermal fluid (Lu 1986; Zhang 1987; Chen 1992; Zhang et al. 1997). Therefore, the mantle end-member in the fluids is most probably exsolved directly from the granitic magma.

The base of stable continental crust is not hot enough to initiate melting. Changes of the thermal regime of normal continental crust may be achieved by two mechanisms (Stuart et al. 1995). Tectonic thickening in collision zones, accomplished by the stacking of thrust sheets and conductive heating from below, may initiate melting of crustal rocks (England and Thompson 1984). Alternatively, a mantle-derived magma intruded the crust causing melting of the crust (Huppert and Sparks 1988). In the first case, helium isotopes of magmatic fluids would be the bulk of the melting crust and will be dominated by crustal radiogenic He. In the latter case, the resulting magma crystallized exsolving a mixture of crustal and mantle helium (Stuart et al. 1995).

As stated above, magmatic fluids differentiated from parental magmas that generated associated granites may have taken part in the formation of the Yaogangxian tungsten deposit. In combination with the geological relationship and the wide range of $^3$He/$^4$He ratios (Table 1), we favor that the mantle helium signatures were probably modified by two processes for the present study. On one hand, the mantle helium from mantle-derived magma which cause melting of the crust was diluted by incorporating radiogenic helium within the parental magma of the associated granite pluton before helium was released into hydrothermal system, a process that could have involved crustal assimilation and magma ageing (Simmons et al. 1987; Stuart et al. 1995; Hu et al. 1998, 2004). On the other hand, the diluted helium in magma fluid emanating from the parental magma, which represents a modified mantle end-member with a $^3$He/$^4$He ratio of ca. 3Ra, the maximum value measured in this study, much less than the typical sub-continental mantle value of ~6 Ra, was diluted once again by radiogenic helium from the crustal fluid (MASW) after the magmatic helium was released into the hydrothermal system.

Early Yanshanian (Jurassic) granitoids, including tungsten mineralization related granites, are widespread in the Nanling region of South China. These granitoids consist mainly of biotite granite, two mica granite and muscovite granite. In most previous studies, they were classified as S-type granites which were interpreted to be derived from the regional Paleoproterozoic meta-sedimentary rocks (e.g. Xu et al. 1984; Lu 1986;

Wang et al. 1989; Hua et al. 2003, 2007, 2010; Chen et al. 2008; Wang 2008; Sun et al. 2009; Wang et al. 2009). Recently, Li et al. (2007a, b, 2009) carried out systematic analysis of in situ zircon Hf-O isotopes, and re-analyzed the geochemical characteristics of a number of representative early Yanshanian Nanling granitoids dated at ca. 155 Ma. The results show that these granitoids are inconsistent with, but transitional between, the typical S- and I-type granites derived respectively from the supercrustal sedimentary rocks and the infracrustal igneous rocks, i.e. products of reworking of meta-sedimentary materials by mantle-derived magmas and mixing between the mantle and supercrustal melts. The helium isotopes of the Yaogangxian deposit provide new lights on the involvement of mantle-derived materials in the genesis of the tungsten deposit related granite.

## Conclusions

The ore-forming fluids of the Yaogangxian tungsten deposit were a mixture between a crustal fluid containing atmospheric Ar and crustal $^{4}He$ and a fluid containing mantle components. The former was a low temperature meteoric fluid which interacted with crustal rocks, and the latter is a fluid exsolved from the W-bearing granitic magma.

The existence of mantle noble gases in fluids, exsolved from the W-bearing granitic magma, provides new insights about the origin of the tungsten deposits and associated granites. The hosting granites were previously considered as S-type, but actually formed by crustal melting induced by intrusion of a mantle-derived magma.

**Acknowledgements** The field work was supported by the Yaogangxian Mine Company. The authors are grateful to Dr. Lehmann B. and Prof. Zhou M.F. for their constructive comments on this manuscript, and to Turner G. and Kendrick M.A. for their thoughtful reviews. This research was financially supported by the National Basic Research Program of China (973 Program) (2007CB411408) and the National Natural Science Foundation of China (40903023).

## References

Ballentine C J, Burnard P G (2002) Production, release and transport of noble gases in the continental crust. Rev Mineral Geochem 47: 481–538

Baptiste PJ, Fouquet Y (1996) Abundance and isotopic composition of helium in hydrothermal sulfides from the East Pacific Rise at 13 N. Geochim Cosmochim Acta 60:87–93

Burnard PG, Polya DA (2004) Importance of mantle derived fluids during granite associated hydrothermal circulation: He and Ar isotopes of ore minerals from Panasqueira. Geochim Cosmochim Acta 68:1607–1615

Burnard PG, Stuart F, Ayliffe L, Turner G (1993) Noble gas isotopic and elemental abundances in inclusion and vesicle trapped fluids: method. Seventh meeting of the European Union of Geosciences. abstract supplement, Seventh meeting of the European Union of Geosciences 5(Suppl. 1):368

Burnard PG, Farley KA, Turner G (1998) Multiple fluid pulses in a Samoan harzburgite. Chem Geol 147:99–114

Burnard PG, Hu RZ, Turner G, Bi XW (1999) Mantle, crustal and atmospheric noble gases in Ailaoshan gold deposit, Yunnan province, China. Geochim Cosmochim Acta 63:1595–1604

Cao XF, Lu XB, He MC, Niu H, Du BF, Mei W (2009) An infrared microscope investigation og fluid inclusions in coexisting quartz and wolframite: a case study of Yaogangxian quartz-vein wolframite deposit. Miner Depos 28:611–620 (in Chinese with English abstract)

Chen YR (1981) Geological features and ore-prospecting indications in the Yaogangxian vein-type tungsten deposit. Geol Prospect 17 (2):25–30 (in Chinese with English abstract)

Chen YR (1992) Analysis of the control fractors and conditions of the mineralization in Yaogangxian orefield, Yizhang county, Hunan. Hunan Geol 11(4):285–293 (in Chinese with English abstract)

Chen J, Lu JJ, Chen WF, Wang RC, Ma DS, Zhu JC, Zhang WL Ji JF (2008) W-Sn-Nb-Ta-bearing granites in the Nanling Range and their relationship to metallogengesis. Geological Journal of China Universities 14: 459–473

Dunai TJ, Baur H (1995) Helium, neon and argon systematics of the European subcontinental mantle: implications for its geochemical evolution. Geochim Cosmochim Acta 59:2767–2784

Elliot T, Ballentine CJ, O'Nions RK, Ricchiuto T (1993) Carbon, helium, neon and argon isotopes in a Po basin natural gas field. Chem Geol 106:429–440

England PC, Thompson AB (1984) Presssure-temperature-time paths of regional metamorphism, I, Heat transfer during evolution of regions of thickened continental crust. J Petrol 25:894–928

Gautheron C, Moreira M (2002) Helium signature of the subcontinental lithospheric mantle. Earth Planet Sci Lett 199:39–47

Guo CL, Wang DH, Che YC, Wang YB, Chen ZH, Liu SB (2007) Precise zircon SHRIMP U-Pb and quartz vein Rb-Sr dating of Mesozoic Taoxikeng tungsten polymetallic deposit in southern Jiangxi. Miner Depos 26:432–442 (in Chinese with English abstract)

Hu RZ, Burnard PG, Turner G, Bi XW (1998) Helium and argon systematics in fluid inclusions of Machangqing copper deposit in west Yunnan province, China. Chem Geol 146:55–63

Hu RZ, Burnard PG, Bi XW, Zhou MF, Peng JT, Su WC, Wu KX (2004) Helium and argon isotope geochemistry of alkaline intrusion-associated gold and copper deposits along the Red River-Jingshajiang fault belt, SW China. Chem Geol 203:305–317

Hu RZ, Burnard PG, Bi XW, Zhou MF, Peng JT, Su WC, Zhao JH (2009) Mantle-derived gaseous components in ore-forming fluids of the Xiangshan uranium deposit, Jiangxi province, China: evidence from He, Ar and C isotopes. Chem Geol 266:86–95

Hua RM, Zhang WL, Chen PR, Wang RC (2003) Comparison in the characteristics, origin, and related metallogeny between granites in Dajishan and Piaotang, Southern Jiangxi, China. Geol J China Univ 9:609–619 (in Chinese with English abstract)

Hua RM, Zhang WL, Gu SY, Chen PR (2007) Comparison between REE granite and W-Sn granite in the Nanling region, South China, and their mineralization. Acta Petrologica Sinica 23:2321–2328 (in Chinese with English abstract)

Hua RM, Li GL, Zhang WL, Hu DQ, Chen PR, Chen WF, Wang XD (2010) A tentative discussion on differences between large-scale tungsten and tin mineralization in South China. Miner Depos 29:9–23 (in Chinese with English abstract)

Huppert HE, Sparks RSJ (1988) The generation of granitic magmas by intrusion of basalt into the continental crust. J Petrol 29:599–624

Jiang GH, Hu RZ, Xie GQ, Zhao JH, Tang QL (2004) K-Ar ages of plutonism and mineralization at the Dajishan tungsten deposit, Jiangxi province, China. Acta Mineralogica Sinica 24:253–256 (in Chinese with English abstract)

Kendrick MA, Burgess R, Pattrick RAD, Turner G (2001) Fluid inclusion noble gas and halogen evidence on the origin of Cu-porphyry mineralizing fluids. Geochim Cosmochim Acta 65:2651–2668

Kendrick MA, Burgess R, Leach D, Pattrick RAD (2002a) Hydrothermal fluid origins in Mississippi valley-type ore districts: combined noble gas (He, Ar, Kr) and halogen (Cl, Br, I) analysis of fluid inclusions from the Illinois-Kentucky fluorspar district, ViburnumTrend and Tri-State districts, Midcontinent United States. Econ Geol 97:453–469

Kendrick MA, Burgess R, Pattrick RAD, Turner G (2002b) Hydrothermal fluid origins in a fluorite-rich Mississippi valley-type district: combined noble gas (He, Ar, Kr) and halogen (Cl, Br, I) analysis of fluid inclusions from the South Pennine ore field, United Kingdom. Econ Geol 97:435–451

Kendrick MA, Burgess R, Harrison D, Bjorlykke A (2005) Noble gas and halogen evidence for the origin of Scandinavian sandstone-hosted Pb-Zn deposits. Geochim Cosmochim Acta 69:109–129

Kendrick MA, Honda M, Oliver NHS, Phillips D (2011) The noble gas systematics of late-orogenic $H_2O$–$CO_2$ fluids, Mt Isa, Australia. Geochim Cosmochim Acta 75:1428–1450

Li XH, Li WX, Li ZX (2007a) On the genetic classification and tectonic implications of the Early Yanshanian granitoids in the Nanling range, South China. Chin Sci Bull 52:1885–1973

Li XH, Li ZX, Li WX, Liu Y, Yuan C, Wei GJ, Qi CS (2007b) U-Pb zircon, geochemical and Sr-Nd-Hf isotopic constraints on age and origin of Jurassic I- and A-type granitoids from central Guangdong, SE China: a major igneous event in response to foundering of a subducted flat-slab? Lithos 96:186–204

Li ZL, Hu RZ, Yang JS, Peng JT, Li XM, Bi XW (2007c) He, Pb and S isotopic constraints on the relationship between the A-type Qitianling granite and the Furong tin deposit, Hunan Province, China. Lithos 97:161–173

Li XH, Li WX, Wang XC, Li QL, Liu Y, Tang GQ (2009) Role of mantle-derived magma in genesis of early Yanshanian granites in the Nanling Range, South China: in situ zircon Hf-O isotopic constraints. Sci China Ser D- Earth Sci 52:1262–1278

Lippolt HJ, Weigel E (1988) $^{4}$He diffusion in Ar-retentive minerals. Geochim Cosmochim Acta 52:1449–1458

Lu HZ (1986) Origin of tungsten mineral deposit in South China. Publishing House of Chongqing, Chongqing, pp 1–232 (in Chinese with English abstract)

Mamyrin BA, Tolstikhin I (1984) Helium isotopes in nature. Elsevier, Amsterdam, pp 267

Mao JW, Xie GQ, Guo CL, Chen YC (2007) Large-scale tungsten-tin mineralization in the Nanling region, South China: metallogenic ages and corresponding geodynamic process. Acta Petrologica Sinica 23:2329–2338 (in Chinese with English abstract)

Marty B, Jambon A, Sano Y (1989) Helium isotope and $CO_2$ in volcanic gases of Japan. Chem Geol 76:25–40

McDougall I, Harrison TM (1988) Geochronology and thermochronology by the $^{40}$Ar-$^{39}$Ar method. Oxford Univ. Press, Oxford, pp 212

Mckee EH, Rytuba J, Xu KQ (1987) Geochronology of the Xihuashan composite granitic body and tungsten mineralization, Jiangxi province, south China. Econ Geol 82:218–223

Morrison P, Pine J (1955) Radiogenic origin of the helium isotopes in rock. Ann N Y Acad Sci 62:71–92

Ni JW (1994) Research on fluid inclusion and ore-forming fluid characters of the Yaogangxian tungsten deposit. J Zhejiang Univ 28:73–81 (in Chinese with English abstract)

Peng JT, Zhou MF, Hu RZ, Shen NP, Yuan SD, BI XW, Du AD, Qu WJ (2006) Precise molybdenite Re-Os and mica Ar-Ar dating of the Mesozoic Yaogangxian tungsten deposit, central Nanling district, South China. Miner Depos 41:661–669

Qiu HN (1996) $^{40}$Ar/$^{39}$Ar dating of the quartz samples from two mineral deposits in western Yunnan (SW China) by crushing in vacuum. Chem Geol 127:211–222

RGNTD (Research Group for Nanling Tungsten Deposits, Chinese Ministry of Metallurgy) (1985) Tungsten Deposits in South China. Publishing House of Metallurgical Industry, Beijing, pp 1–496 (in Chinese with English abstract)

Simmons SF, Sawkins FJ, Schlutter DJ (1987) Mantle-derived helium in two Peruvian hydrothermal ore deposits. Nature 329:429–432

Smith PE, Evensen NM, York D, Szatmari P, Oliveira DC (2001) Single-crystal $^{40}$Ar/$^{39}$Ar dating of pyrite: no fool's clock. Geology 29:403–406

Stuart FM, Turner G, Duckworth RC, Fallick AE (1994) Helium isotopes as tracers of trapped hydrothermal fluids in ocean-floor sulfides. Geology 22:823–826

Stuart FM, Burnard PG, Taylor RP, Turner G (1995) Resolving mantle and crustal contributions to ancient hydrothermal fluids: He-Ar isotopes in fluid inclusions from Dae Hwa W-Mo mineralisation, South Korea. Geochim Cosmochim Acta 59:4663–4673

Sun J, Ni YJ, Bai DY, Ma TQ (2009) Geochemistry, petrogenesis and tectonic setting of early Yanshanian Yaogangxian granite pluton, Southeastern Hunan province (in Chinese with English abstract). Geology and Mineral Resources in South China (3):12–18

Torgersen T, Kennedy BM, Hiyagon H (1988) Argon accumulation and the crustal degassing flux of $^{40}$Ar in the Great Artesian Basin, Australia. Earth Planet Sci Lett 92:43–59

Turner G, Stuart FM (1992) Helium/heat ratios and deposition temperatures of sulphides from the ocean floor. Nature 357:581–583

Turner G, Wang SS (1992) Excess argon, crustal fluid and apparent isochrons from crushing K feldspar. Earth Planet Sci Lett 110:193–211

Turner G, Burnard PG, Ford JL, Gilmour JD, Lyon IC, Stuart FM (1993) Tracing fluid sources and interaction. Phil Trans R Soc Lond, A 344:127–140

Wang Y (2008) Some further discussion on the granitic types of the Early Yanshanian (Jurassic) granitoids in the Nanling area, SE China. Geol Rev 54:162–174 (in Chinese with English abstract)

Wang LK, Zhang SL, Yang WJ, Xu WX (1989) Granites of different series and types in South China: their Sr, O, Pb and Nd isotopic compositions and formation environment. Geol Prospect 25:29–33 (in Chinese with English abstract)

Wang QY, Hu RZ, Peng JT, Bi XW, Wu LY, Liu H, Su BX (2007) Characteristics and significance of the fluid inclusions from Yaogangxian tungsten deposit in south Hunan. Acta Petrologica Sinica 23:2263–2273 (in Chinese with English abstract)

Wang YL, Per RF, Li JW, Liu XF (2009) Geochemical characteristics of granites from the Jiangjunzhai tungsten deposit of Southeast Hunan province and its Re-Os isotopic dating. Rock Miner Anal 28:274–278 (in Chinese with English abstract)

Wu LY, Hu RZ, Peng JT, Bi XW, Jiang GH, Chen HW, Wang QY, Liu YY (2011) He and Ar isotopic compositions and genetic implications for the giant Shizhuyuan W-Sn-Bi-Mo deposit, Hunan Province, South China. Int Geol Rev 53:677–690

Xiao J, Wang Y, Hong YL, Zhou YZ, Xie MH, Wang DS, Guo JS (2009) Geochemistry characteristics of Xihuashan tungsten granite and its relationship to tungsten metallogenesis. J East China Inst Technol 32:22–31 (in Chinese with English abstract)

Xu KQ, Sun N, Wang DZ (1984) Petrogenesis of the granitoids and their metallogenetic relations in south China. In: Xu KQ, Tu GC (eds) Geology of granites and their metallogenetic relations. Science Press, China, pp 1–31

Yan D P, Zhou M F, Song H L, Wang X W, Malpas J (2003) Origin and tectonic significance of a Mesozoic multi-layer over-thrust system within the Yangtze Block (South China). Tectonophysics, 361: 239–254

York D, Masliwec A, Kuybida P, Hanes JE, Hall CM, Kenyon WJ, Spooner ETC, Scott SD (1982) $^{40}$ Ar/$^{39}$ Ar dating of pyrite. Nature 300:52–53

Zhang LG (1987) Oxygen isotopic studies of wolframite in tungsten ore deposits of South China. Geochimica 3:233–242 (in Chinese with English abstract)

Zhang GX, Xie YN, Yu FJ, Zhang HB (1997) Stable isotope geochemistry of different metallogenic stages of tungsten deposit in Dajishan mine. Jiangxi 18(suppl):197–199 (in Chinese with English abstract)

Zhang WL, Hua RM, Wang RC, Chen PR, Li HM (2006) New dating of the Dajishan granite and related tungsten mineralization in Southern Jiangxi. Acta Geologica Sinica 80:956–962 (in Chinese with English abstract)

Zhang WL, Hua RM, Wang RC, Li HM, Qu WJ, Ji JQ (2009) New dating of the Piaotang granite and related tungsten mineralization in southern Jiangxi. Acta Petrologica Sinica 83:659–670 (in Chinese with English abstract)